Single-agent nintedanib suppresses metastatic osteosarcoma growth by inhibiting tumor vascular formation

TAKATSUNE SHIMIZU[1], ATSUNOBU SAGARA[2], YUMI FUKUCHI[1] and AKIHIRO MUTO[1]

[1]Department of Pathophysiology, School of Pharmacy and Pharmaceutical Sciences;
[2]Division of Applied Pharmaceutical Education and Research, Hoshi University, Tokyo 142-8501, Japan

Abstract. New therapeutic approaches are needed for osteosarcoma, which is the most common malignancy of the bone, especially for metastatic cases. Nintedanib is a potent, oral tyrosine kinase inhibitor approved for treating idiopathic pulmonary fibrosis, which blocks a variety of receptor signals, including fibroblast growth factor receptors, vascular endothelial growth factor receptors and platelet-derived growth factor receptors. The present study assessed the effect of nintedanib on previously developed mouse AXT osteosarcoma cells, and on AXT-derived osteosarcoma developed in C57BL/6 mice, which displays lethal tumors with osteoid formation and lung metastatic lesions that mimics human disease. *In vitro* analysis, including flow cytometry and immunoblotting, revealed that nintedanib inhibited AXT cell proliferation and cell cycle progression, induced apoptosis, and inactivated AKT and ERK1/2. Immunoblot analysis using tumor lysates demonstrated that nintedanib inhibited its target molecules *in vivo*. As a single agent, nintedanib decreased the size of primary AXT-derived osteosarcoma, and reduced circulating tumor cells and lung metastasis. Immunohistochemical findings indicated that nintedanib exerted antitumor activity mainly by inhibiting the formation of CD31-positive tumor vasculature, while αSMA-positive cells were still enriched in tumors after nintedanib treatment. In addition, nintedanib exhibited an anti-osteosarcoma effect on C57BL/6 severe combined immunodeficient mice in which T- and B-cell function is obsolete, suggesting that the antitumor effect of nintedanib was not attributable to antitumor immunity. Collectively, these findings indicated that nintedanib holds potential for treating osteosarcoma.

Correspondence to: Dr Takatsune Shimizu, Department of Pathophysiology, School of Pharmacy and Pharmaceutical Sciences, Hoshi University, 2-4-41 Ebara, Shinagawa-ku, Tokyo 142-8501, Japan
E-mail: t-shimizu@hoshi.ac.jp

Introduction

Osteosarcoma is the most common primary bone tumor in childhood and adolescence. Recent progresses in treatment consisting of surgery and adjuvant chemotherapy have improved prognosis. However, still ~30% of patients do not have long-term survival, mainly due to uncontrollable metastasis (1-4). Thus, novel and safe solutions for overcoming therapeutic resistance must urgently be developed.

Previously, we established a mouse osteosarcoma model using bone marrow stromal cells derived from *Ink4a/Arf* null mice by overexpression of c-MYC (5). When these osteosarcoma cells, designated AXT cells, were inoculated into C57BL/6 syngeneic mice, lethal tumors with metastatic lesions rapidly develop that mimic the pathophysiology of human osteoblastic osteosarcoma (6-9). Since osteosarcoma develops from mesenchymal origin, agents that suppress the function of mesenchymal cells such as fibroblasts might also exert anti-osteosarcoma *in vivo*.

Nintedanib (formerly known as BIBF 1120) is an oral small-molecule anti-fibrotic drug that is a triple angiokinase inhibitor; the drug inhibits fibroblast growth factor (FGF), vascular endothelial growth factor (VEGF), and platelet-derived growth factor (PDGF) signaling pathways (10-12). Nintedanib is FDA-approved for treating idiopathic pulmonary fibrosis (IPF) and advanced lung adenocarcinoma (12-15). Preclinical *in vitro* and *in vivo* studies have shown that nintedanib exerts an anti-tumor effect in various types of cancers including non-small cell lung cancer, renal cell carcinoma, cholangiocarcinoma, colorectal cancer, ovarian cancer, prostate cancer, and pancreatic ductal adenocarcinoma (10,16-18). Importantly, in addition to directly targeting malignant tumor cells, nintedanib exerts an anti-tumor effect by increasing the sensitivity of the tumor to other anti-tumor drugs and affecting the tumor microenvironment (16,18-20). The influence of nintedanib on the microenvironment suppresses the function of cancer-associated fibroblasts (CAFs) that critically support cancer progression (21-23). Therefore, *in vitro* studies alone are not sufficient to evaluate the anti-tumor effect of nintedanib and *in vivo* studies are needed. Clinically, in addition to benefits in non-small cell lung cancer, nintedanib has efficacy in ovarian cancer and mesothelioma either as adjuvant therapy after chemotherapy or in combination with chemotherapy (24,25).

A previous study showed that nintedanib suppresses lung metastasis of osteosarcoma cells by inhibiting fibrotic remodeling of osteosarcoma stem cells, suggesting that nintedanib is useful for treating osteosarcoma metastasis (26). However, the anti-tumor effect of nintedanib in osteosarcoma has not been fully elucidated. In this study, the clinical potential of nintedanib for treating osteosarcoma was examined *in vitro* and in a mouse model that mimics human disease, and the molecular mechanisms of nintedanib activity were examined.

Materials and methods

Cell culture. Mouse osteosarcoma AXT cells, which were previously established from *Ink4a/Arf*-null mice by overexpression of human c-MYC (5), or human osteosarcoma cells (U2OS (#HTB-96), MG63 (#CRL-1427), Saos2 (#HTB-85) purchased from ATCC (Manassas, VA, USA) were cultured in IMDM (Nacalai Tesque, Kyoto, Japan) or McCoy's 5A medium (Thermo-Fischer Scientific, Carlsbad, CA, USA), respectively, containing 10% FBS under 5% CO_2 at 37°C (27,28). Mouse bone marrow stromal cells (wild-type or Ink4a/Arf null BMSCs) were established as previously described (5). Briefly, bone marrow cells from C57BL/6J or Ink4a/Arf null mice were collected from femurs and tibias and hematopoietic cells were depleted with antibodies to CD45 and lineage-specific antigens. Adherent cells were cultured in IMDM supplemented with 20% FBS and used as BMSCs within ten passages.

Reagents. Nintedanib (#HY-50904 MedChemExpress, Monmouth Junction, NJ, USA) was dissolved in dimethyl sulfoxide (DMSO) at a stock concentration of 20 mM.

Cell viability evaluation. AXT cells or human osteosarcoma MG63, Saos2, and U2OS cells ($5x10^2$ in 50 μl of IMDM for AXT cells or McCoy's 5A medium for MG63, Saos2, and U2OS cells, containing 10% FBS) were cultured in a 96-well cell culture plate. Then, 50 μl of the corresponding medium containing test reagents at twice the desired concentrations was added to each well. Cell viability was evaluated using a Cell Titer Glo assay kit (Promega, Madison, WI, USA). Assays were performed at least in triplicate and data are shown as the means ± SD relative (fold) against the corresponding control value for cells incubated in the absence of test reagents.

Endothelial cell tube formation assay. A 96-well cell culture plate was coated with 30 μl of Matrigel (Corning, Corning, NY, USA) and Human Umbilical Vein Endothelial Cells (HUVEC (#KE-4109) purchased from CRABO, Osaka, Japan) cultured with Endothelial Cell Growth Medium (Takara, Shiga, Japan) were seeded after passing through the 40 mm-cell strainer ($2x10^4$ in 45 μl of the culture medium per each well). Then, 25 μl of the culture medium with or without 400 nM or 4 μM of nintedanib was added and the final total volume was 100 μl. Tube formation was evaluated after 14 h.

Mouse care. All mouse experiments were performed in accordance with the guidelines of Hoshi University, and the present study was approved by the Committee on Animal Research of Hoshi University (approval number: 20-071). Mice were housed in ventilated cages (five mice/cage; floor area 501 cm^2) under specific pathogen-free conditions. Mice were fed a standard chow diet and water *ad libitum*. Rooms were maintained at 22°C and kept on a 12 h light and dark cycle with inspection every weekday to ensure that they were not under distress throughout the experiments.

Tumor xenograft model. The detailed duration of the experiments and the number of animals used was shown in main figures. Briefly, $1\text{-}2x10^6$ AXT cells were suspended in 100 μl of IMDM and injected subcutaneously into the bilateral flanks (two injections in total) of 7-week-old female C57BL/6J mice (SLC, Shizuoka, Japan) or 20-week-old female C57BL/6 SCID mice (The Jackson Laboratory, Bar Harbor, ME, USA) under inhalation anesthesia with 4% isoflurane (Wako, Tokyo, Japan) for the induction and 2% for maintenance.

Nintedanib at 50 mg/kg was orally administered once a day. The endpoint criteria were as follows: i) The mean tumor diameter exceeds 20 mm. ii) The combined tumor burden is more than 15% of body weight (~20 g of 7-week-old mice). iii) Occurrence of ulceration, infection, or necrosis of tumor. iv) Body weight loss is more than 20% of weight. The results did not reach the endpoint criteria in this study. Bilateral two tumors developed in each mouse in this study. The major and minor axes of the bilateral tumors were measured, and the estimated tumor volume was calculated according to the guideline of Washington State University (https://iacuc.wsu. edu/documents/2017/12/tumor-burden-guidelines.pdf/).

Estimated tumor volume $(mm^3)=d^2 \times D/2$. D and d were the major and minor diameter in mm, respectively. The maximum diameter and the volume of bilateral tumors observed in each mouse was listed in Table SI. When the mice were euthanized, a lethal dose (200 mg/kg) of pentobarbital sodium (Tokyo Kasei Kogyo, Tokyo, Japan) was intraperitoneally injected. Death was confirmed by cardiac arrest. None of the mice was unexpectedly dead or found dead during the study.

Immunoblot analysis. 2X Laemmli sample buffer (Bio-Rad, Hercules, CA, USA) supplemented with β-mercaptoethanol was used for the preparation of cell lysate. Immunoblot analyses were performed according to standard semi-dry transfer methods using 5-20% gradient precast polyacrylamide gels (ePAGEL, ATTO, Tokyo, Japan). The primary antibodies were listed in Table SII. Signal intensities were quantitated using the ImageJ software (29), and the relative (fold) values against the corresponding control value normalized against the intensities of the α-Tubulin bands are shown.

Phospho-kinase array. Activated tyrosine kinase *in vivo* was screened using the mouse RTK phosphorylation antibody array C1 kit (RayBiotech, Norcross, GA, USA). The array map is shown in Table SIII. AXT cells were inoculated into C57BL/6J mice and nintedanib was administrated. The tumor lysate from two tumors of two mice was extracted by disruption using a BioMasher homogenizer (Nippi, Tokyo, Japan). The total cell lysate used was 500 μg.

Cell-cycle analysis. Trypsinized cells were washed with PBS, fixed with 70% ethanol for ≥48 h at -20°C, washed twice with ice-cold PBS, and stained with PBS supplemented with
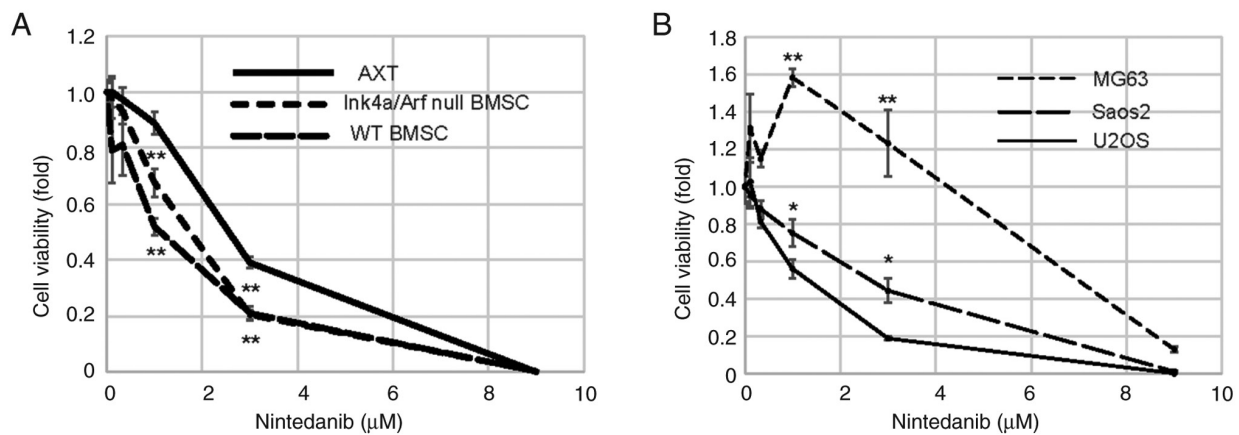
Figure 1. Nintedanib inhibits the viability of osteosarcoma cells. (A) The viability of AXT and BMSC from Ink4a/Arf null mice and WT C57BL/6 mice was measured after 3 day exposure to the indicated concentrations of nintedanib. Data are shown as the means ± SD relative to the corresponding value without nintedanib exposure. *P<0.05, **P<0.005 vs. AXT. (B) The viability of MG63, Saos2, and U2OS cells treated with the indicated concentrations of nintedanib for 3 days. Data are shown as the means ± SD from quadruplicate experiments relative to the corresponding value without nintedanib exposure. *P<0.05, **P<0.005 vs. U2OS. BMSC, bone marrow stromal cells; WT, wild-type.

10 μg/ml propidium iodide and 20 μg/ml RNase. The DNA content of 20,000 singlet cells was measured by FACSVerse (BD Biosciences, San Jose, CA, USA).

Evaluation of apoptosis by flow cytometry. Trypsinized cells were washed with ice-cold PBS, and stained with allophycocyanin-conjugated annexin V (eBioscience, Carlsbad, CA, USA) and propidium iodide. Stained cells were analyzed by FACSVerse. FlowJo software (Tree Star, Ashland, OR, USA) was used for the data management.

Reverse transcription (RT) and quantitative (q)PCR analysis. Total RNA was extracted and RT and qPCR analyses were performed using the NucleoSpin RNA kit and PrimeScript (Takara). To evaluate circulating tumor cells (CTCs), whole blood was collected from the right ventricle of euthanized mice and total RNA was extracted from 200 μl blood with a NucleoSpin RNA blood kit (Takara, Shiga, Japan). Since GFP is constitutively expressed in AXT cells, CTCs were quantitated based on the expression level of *Gfp* relative to *Actb* mRNA. The sequences of PCR primers are as follows: *GFP* forward: 5'-GACGTAAACGGCCACAAGTT-3', reverse: 5'-TTGCCG GTGGTGCAGATGAA-3', *Ccnd1* forward: 5'-CAACAACTT CCTCTCCTGCT-3', reverse: 5'-ACTCCAGAAGGGCTT CAATC-3', *Actb* forward: 5'-CAACCGTGAAAAGATGAC CC-3', reverse: 5'-TACGACCAGAGGCATACAG-3'. qPCR analysis was performed with StepOne thermal cycler (Thermo Fisher Scientific) with the 2-step protocol; 60 sec at 95˚C, then 40 cycles of 15 sec at 95˚C and 60 sec at 60˚C followed by the melting and dissociation curve analysis.

Immunohistochemistry (IHC). Immunohistochemical analysis was performed according to standard procedures (5,6,8). Deparaffinized sections were stained with primary antibodies listed in Table SII. Hematoxylin was used for nuclear staining.

Immunofluorescence. Deparaffinized tumor sections were stained with primary antibodies to aSMA (Abcam) derived from rabbit and to CD31 (eBiosience) derived from rat. Alexa

Fluor 555-conjugated anti-rabbit and Alexa Fluor 647-conjugated anti-rat secondary antibody (both from Abcam) were used. DAPI solution (Dojindo, Kumamoto, Japan) was used for nuclear staining. Samples were observed with FV3000 confocal microscopy (Olympus, Tokyo, Japan).

Statistical analysis. Unless indicated otherwise, quantitative data are expressed as the means ± SD relative to the control value. All assays were performed at least in triplicate. Data were analyzed with a Student's t-test or one-way analysis of variance (ANOVA) with the Dunnet post hoc test, using Graph Pad Prism 9 (GraphPad Software, San Diego, CA, USA). P<0.05 was considered to indicate a statistically significant difference.

Results

Nintedanib suppresses osteosarcoma cell growth. First, the anti-proliferative effect of nintedanib on osteosarcoma cells *in vitro* was evaluated. Nintedanib decreased the viability of mouse osteosarcoma AXT cells in a concentration-dependent manner (Fig. 1A). To examine the effect of nintedanib on the non-tumor counterparts of AXT cells, Ink4a/Arf null BMSC and wild-type BMSC derived from the C57BL/6 background were used (5). The growth of both cell lines was also inhibited by nintedanib in a concentration-dependent manner and these cell lines were more sensitive to nintedanib than AXT cells (Fig. 1A). Next, the anti-proliferative effect of nintedanib on human osteosarcoma cells was evaluated. Similar to findings with AXT cells, nintedanib had a direct anti-proliferative effect on human U2OS and Saos2 osteosarcoma cells, but the effect of the drug on MG63 cells was less pronounced (Fig. 1B) and concentrations of nintedanib ≤3 μM did not suppress growth. These results indicate that the effect of nintedanib in osteosarcoma is dependent on cell type *in vitro*.

Nintedanib suppresses cell-cycle progression and survival signals in osteosarcoma cells. To elucidate the mechanisms underlying the suppression of osteosarcoma cell growth by nintedanib, the cell-cycle status was examined. A 20 h
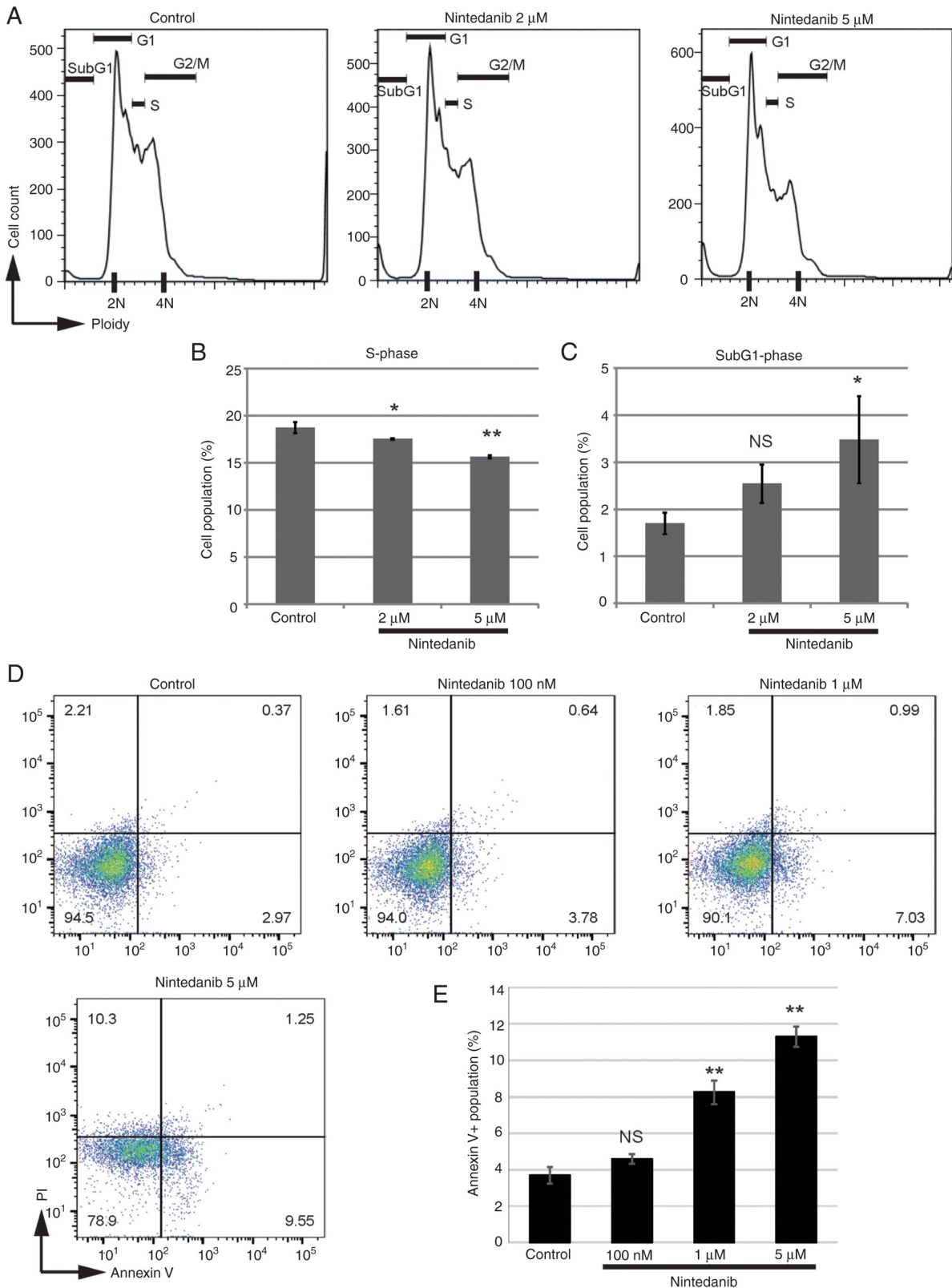
Figure 2. The effect of nintedanib on the cell cycle and induction of apoptosis. (A and B) DNA content in AXT cells treated with the indicated concentrations of nintedanib for 20 h was analyzed by flow-cytometry. The size of S-phase or SubG1 fraction of cells is shown in (B) and (C), respectively. (D) AXT cells were treated with the indicated concentrations of nintedanib for 23 h, and then stained with annexin V and propidium iodide. The representative dot plots including each value on the quadrant are shown. (E) The corresponding ratio of annexin V+ cells in triplicate experiments was also shown. *P<0.05, **P<0.005 vs. control.

exposure of AXT cells to nintedanib decreased the fraction in S-phase (Fig. 2A and B). Treatment with nintedanib increased the sub-G1 fraction (Fig. 2C), indicating the

emergence of apoptotic cells. To further evaluate the induction of apoptosis, AXT cells were treated with nintedanib for 23 h. Although the level of annexin V-positive apoptotic cells
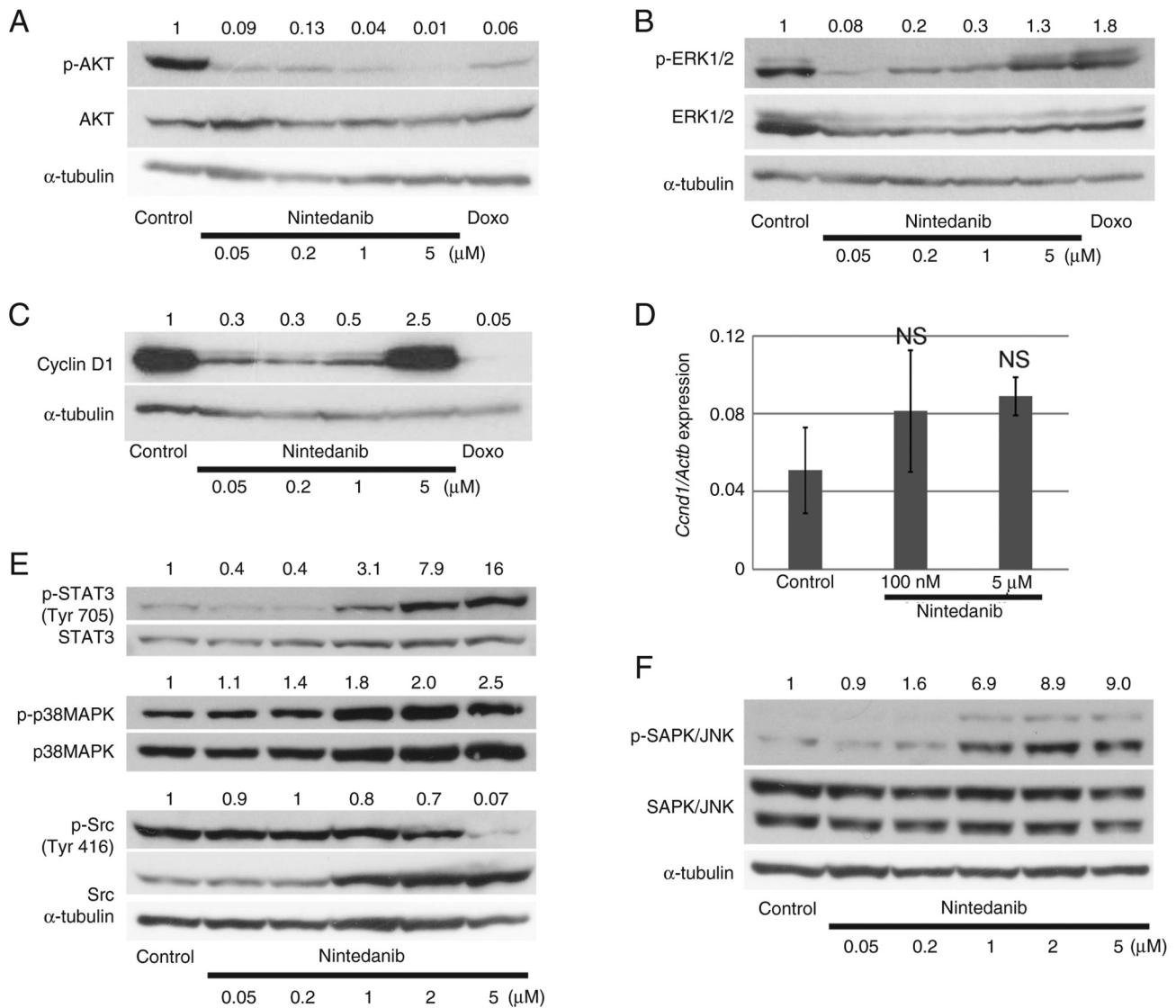
Figure 3. The effect of nintedanib on signaling molecules in AXT cells. (A) Immunoblot analysis of p-AKT and AKT in AXT cells treated with the indicated concentrations of nintedanib or 200 nM Doxo for 21.5 h. (B) Immunoblot analysis of p-ERK1/2 and ERK1/2 under the same conditions as in (A). (C) Immunoblot analysis of CyclinD1 under the same conditions as in (A). The relative (fold) values of p-AKT, p-ERK and Cyclin D1 against the corresponding control value normalized against the intensities of the a-Tubulin bands are shown. (D) Reverse transcription and quantitative PCR analysis of *Ccnd1* mRNA in AXT cells treated with the indicated concentrations of nintedanib for 17 h. Data are normalized against the corresponding expression levels of *Actb* mRNA and are the means ± SD of triplicate experiments. (E) Immunoblot analysis of the respective molecule in AXT cells treated with the indicated concentrations of nintedanib for 24 h. (F) Immunoblot analysis of p-JNK and JNK under the same conditions as in (E). The relative (fold) values of p-STAT3, p-p38, p-Src and p-JNK against the corresponding control value normalized against the intensities of the α-Tubulin bands are shown. Doxo, doxorubicin; NS, not significant; p-, phosphorylated.

was not high, nintedanib concentration-dependently increased the percentage of this cell type (Fig. 2D and E). Together, these findings suggest that nintedanib inhibited cell-cycle progression and increased apoptotic cells in AXT cells.

To clarify the molecular events induced by nintedanib treatment, we evaluated activated kinases by immunoblotting. Phosphorylation of AKT was decreased by 21.5 h treatment with nintedanib or doxorubicin as a positive control (Fig. 3A). The phosphorylation level of ERK1/2 was also attenuated by nintedanib treatment. However, this suppression was not concentration-dependent and ERK1/2 activation was restored by 5 μM nintedanib treatment (Fig. 3B). The expression level of cyclin D1 was downregulated by nintedanib treatment. Notably, similar to the ERK1/2 phosphorylation result, 5 μM

nintedanib restored cyclin D1 protein levels to control values (Fig. 3C). Cells treated with 5 μM nintedanib had higher gene expression levels of cyclin D1 than controls, but the level was not statistically significant (Fig. 3D). Thus, the high expression level of cyclin D1 induced by 5 μM nintedanib could be mainly attributable to the accumulation of cyclin D1 protein.

We further examined the activation of signaling molecules downstream of growth factor or cytokine receptors such as IL-6 and CXCL8 which are suggested to be important to promote osteosarcoma metastasis (30-32). Phosphorylation level of STAT3 was not high under the culture with 10% FBS containing medium and tended to be suppressed only at low concentration of nintedanib like p-ERK (Fig. 3E). p38MAPK and SAPK/JNK were activated by the supplement
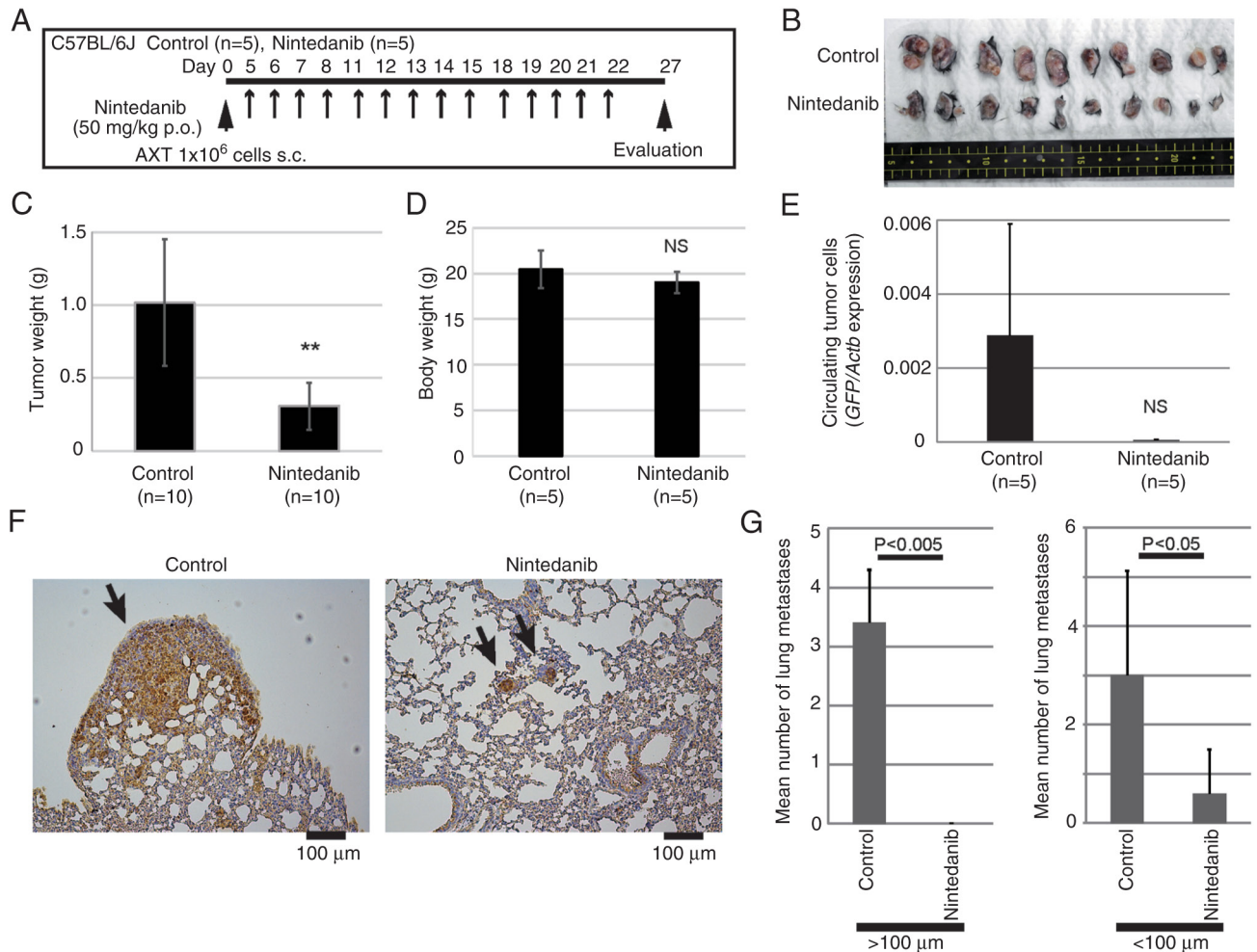
Figure 4. The anti-osteosarcoma activity of nintedanib *in vivo*. (A) A schedule showing cell transplantation and drug administration. (B) Excised tumors in control mice or mice receiving nintedanib. (C) The weight of the tumors. Data are shown as the means ± SD. **P<0.005 vs. control. (D) The weight of control mice or mice receiving nintedanib. Data are shown as the means ± SD. (E) Reverse transcription and quantitative PCR analysis of *GFP* expression in whole blood derived from control mice or mice receiving nintedanib. Data are normalized against the corresponding expression level of *Actb* mRNA and are shown as the means ± SD. (F) Representative images of lung metastases stained with GFP. The arrows indicate lung metastatic lesions. (G) The lung metastases were classified according to whether the major axis was larger than 100 µm. Then, the number of metastatic lesions present throughout a randomly sliced section was counted. Data were shown as the mean values ± SD from the right lungs of five mice.

of nintedanib (Fig. 3E and F). These molecules might not be activated as downstream of cytokine or growth factor receptors. On the other hand, Src was inactivated by the supplement of high concentration of nintedanib, consistent with a previous report that nintedanib suppresses many kinases related to Src activation at high concentrations (10).

Collectively, these results showed that nintedanib altered the expression levels of intracellular signaling molecules, but the effect of nintedanib on these molecules was not necessarily concentration-dependent.

Anti-osteosarcoma effect of nintedanib in vivo. We examined whether nintedanib might exert anti-tumor activity against AXT cells *in vivo*. AXT cells were inoculated into syngeneic C57BL/6 mice and then the mice were treated with a single daily dose of nintedanib at 50 mg/kg (Fig. 4A). Previous toxicity tests using mice reported that no major adverse events occurred when daily 100 mg/kg nintedanib was orally administered for 14 days, and the approximate lethal single dose is over 2,000 mg/kg. The *in vivo* studies using mouse IPF models

demonstrated that a daily dose of 24.9-83 mg/kg nintedanib in mice was efficacious and tolerated when administered for 10 to 30 days (URL: [Ofev, INN-nintedanib (europa. eu)], [https://www.ema.europa.eu/en/documents/assessment-report/ofev-epar-public-assessment-report_en.pdf]). Therefore, we set 50 mg/kg of nintedanib to evaluate the anti-tumorigenic effect.

Administration of nintedanib significantly decreased the primary tumor size and weight (Fig. 4B and C). Treatment with nintedanib did not affect the mouse body weight (Fig. 4D) and all mice were alive, well, and not exhausted during the treatment. Since AXT cells were labeled with GFP, circulating tumor cells could be quantitated (27,28). Treatment with nintedanib decreased the number of circulating tumor cells, although the effect was not statistically significant (Fig. 4E). Consistent with those findings, nintedanib also significantly reduced the levels of lung metastatic lesions (Fig. 4F and G). Notably, large metastatic lesions over 100 µm diameter were not detected in nintedanib-treated mice.
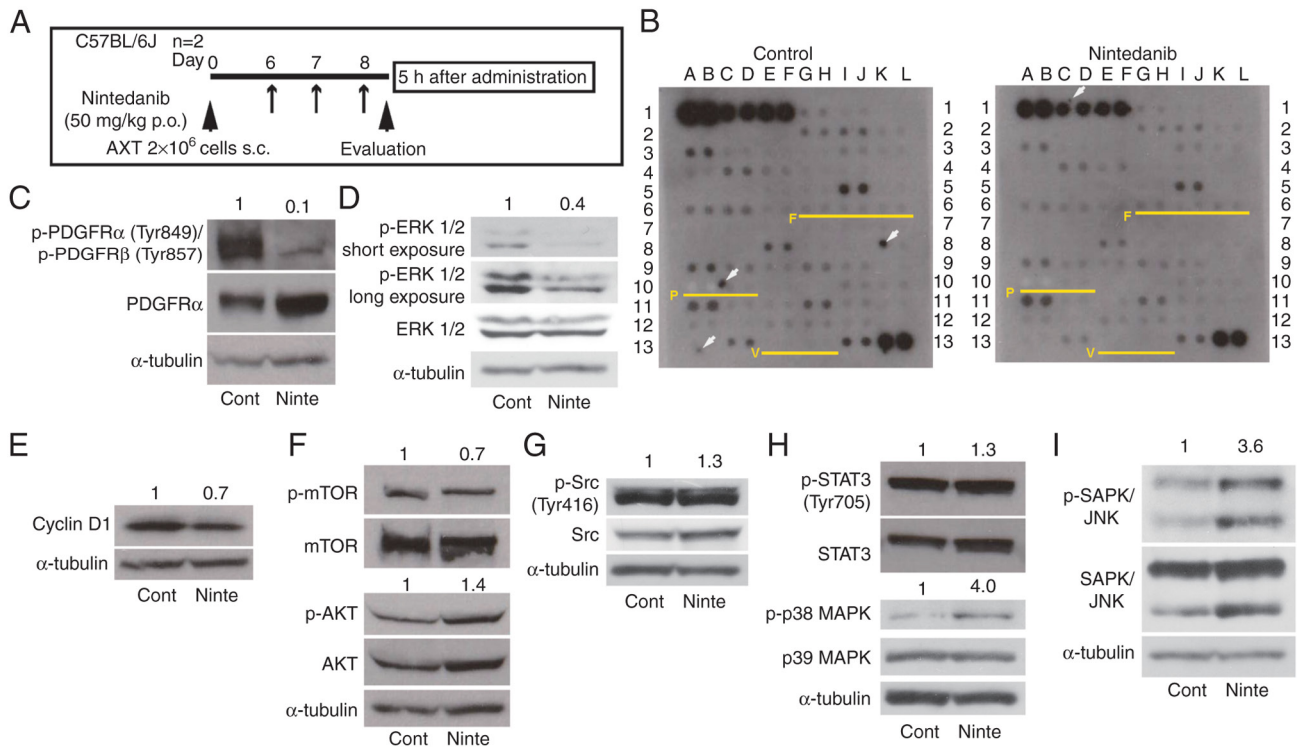
Figure 5. Kinase activation in AXT cells with treatment of nintedanib *in vivo*. (A) A schedule of cell transplantation and nintedanib administration. (B) Tumor lysates were prepared from mice treated with or without nintedanib. Protein (500 μg per sample) was analyzed on a mouse phospho-receptor tyrosine kinase array. Each antibody was spotted in duplicate. The array map is shown in Table SIII. F: FGFRs, P: PDGFRs, V: VEGFR2/3. White arrows: nonspecific spots. Immunoblot analysis of (C) p-PDGFRs and PDGFRa, (D) p-ERK1/2 and ERK1/2, (E) CyclinD1, (F) p-mTOR, mTOR, p-AKT and AKT, (G) p-Src and Src, (H) p-STAT3, STAT3, p-p38 MAPK and p38 MAPK, and (I) p-JNK and JNK using the same tumor lysate analyzed in (B). The relative (fold) values of the phosphorylated forms of indicated molecules and Cyclin D1 against the corresponding control value normalized against the intensities of the α-Tubulin bands are shown. p-, phosphorylated.

Therefore, these findings show that nintedanib as a single agent exerted an anti-tumor effect on primary lesions and metastatic growth of osteosarcoma.

Nintedanib attenuates PDGFR activation in vivo. To elucidate the molecular mechanisms underlying the anti-osteosarcoma effect *in vivo*, tumor lysate was prepared from tumors developed in mice inoculated with AXT cells as shown in Fig. 5A, and then the phosphorylation levels of receptor tyrosine kinases per unit of protein were compared. Phosphorylation was still detected in 31 of 71 kinases in the lysate from nintedanib-treated mice (Fig. 5B). FGFR, PDGFR, and VEGFR are the molecular targets for nintedanib (10-12), but phosphorylation levels of FGFR1 and FGFR2 were very weak and not affected by nintedanib treatment. Activation of PDGFRα/β, VEGFR2, and VEGFR3 could not be detected using this phosphorylation array system.

To further evaluate the activation levels of PDGFRs and VEGFR2, the same lysate was subjected to immunoblotting. The activation of PDGFRα/β was attenuated by nintedanib administration (Fig. 5C), suggesting that nintedanib inhibited its molecular targets *in vivo*. Phosphorylation of Tyr951 or Tyr996 of VEGFR2 was not detected (data not shown). We examined the activation status of downstream molecules. Consistent with our *in vitro* results at low concentrations, nintedanib decreased ERK1/2 phosphorylation levels (Figs. 3B and 5D). Cyclin D1 was slightly downregulated (Fig. 5E). However, phosphorylation levels of mTOR and AKT were not affected by nintedanib (Fig. 5F).

We evaluated the activation of PDGFR in AXT cells *in vitro* and compared to the result from the *in vivo* samples (Fig. S1A). Our previous studies using immunoprecipitation western blotting showed that PDGFR activation was difficult to detect under the culture with FBS containing medium without supplement of PDGF ligands (7). In addition, under the presence of serum *in vitro*, survival of AXT cells was not dependent on the PDGFR signaling. Consistent with our previous findings, the activation of PDGFR *in vitro* was considerably weaker than that *in vivo*. Interestingly, the expression level of PDGFRα increased with nintedanib treatment, but the associated receptor activation was not observed (Fig. S1B). In *in vivo* tumor samples, phosphorylation status of Src and STAT3 was not attenuated by nintedanib administration (Fig. 5G and H). On the other hand, like *in vitro* results, p38MAPK and SAPK/JNK were activated by nintedanib administration (Figs. 3E, F, 5H and I). These results suggest that nintedanib does not block STAT3 signaling under 50 mg/kg administration, and p38MAPK and SAPK/JNK might not be activated as downstream of cytokine or growth factor receptors.

Nintedanib suppresses tumor vasculature formation but does not inhibit the enrichment of αSMA-positive cells to osteosarcoma. To clarify nintedanib-mediated histological changes and the mechanisms underlying anti-osteosarcoma effect *in vivo*, immunohistochemical analyses were performed.
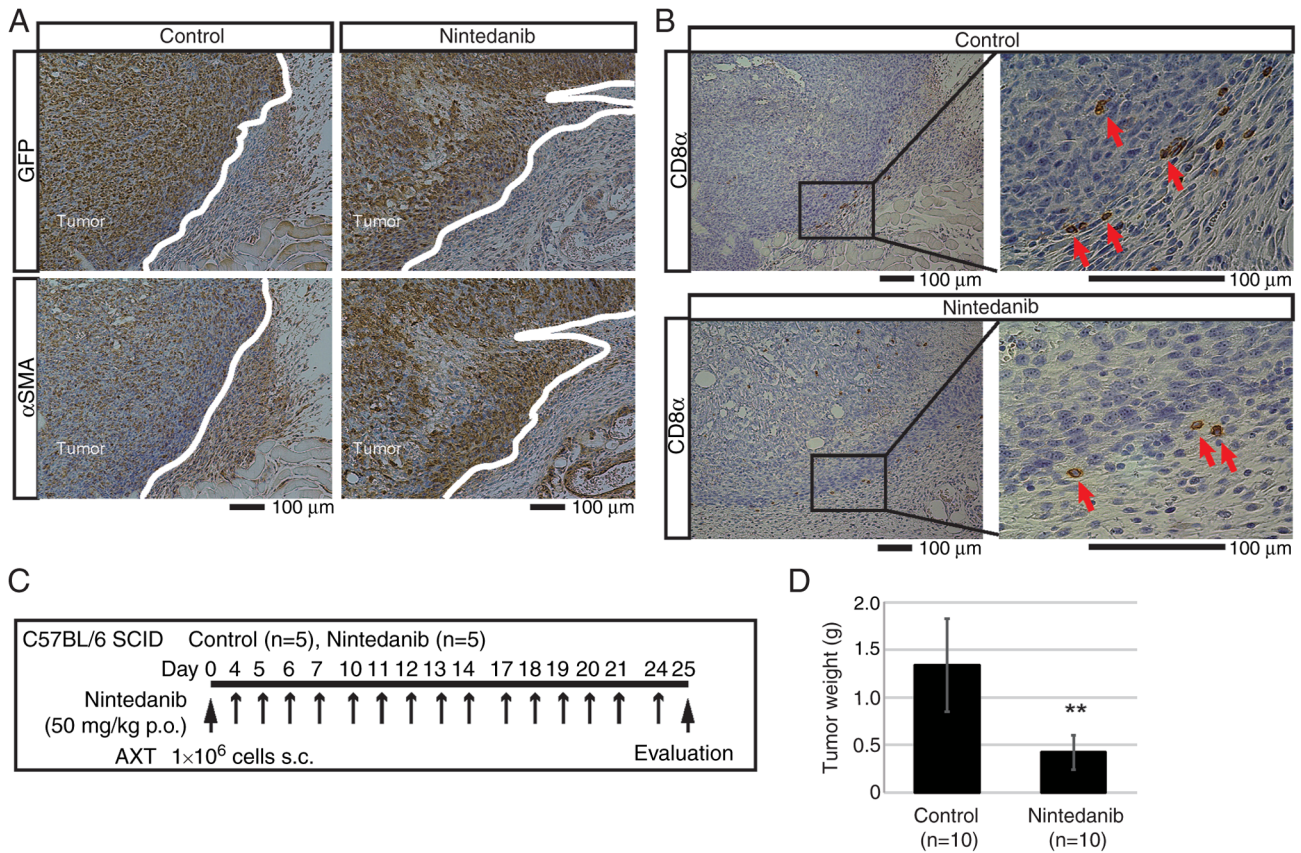
Figure 6. The effect of nintedanib on αSMA-positive cells and tumor immunity. (A) Representative serial section images of an AXT-derived osteosarcoma stained with GFP and αSMA antibody. Tumor margins are shown as white lines. Tumors were developed according to the schedule in Fig. 4A. (B) Representative images of an AXT-derived osteosarcoma stained with CD8α antibody. The arrows indicate CD8α-positive cells. Boxed regions highlight the magnified images. (C) The schedule of cell inoculation and nintedanib administration in C57BL/6 SCID mice. (D) Weight of tumors developed in C57BL/6 SCID control mice or mice receiving nintedanib. [**]P<0.005 vs. control. Data are shown as the means ± SD. αSMA, α-smooth muscle actin.

Previous reports suggest that nintedanib exerts anti-tumor activity by inhibiting the functions of CAFs or fibrogenic reprogramming that confers to metastatic ability to osteosarcoma cells (21,22,26). α-smooth muscle actin (αSMA) is a useful marker for smooth muscle cells and a part of fibroblasts including myofibroblasts or CAFs (33,34). In osteosarcoma developed according to Fig. 4A, αSMA positive cells consisted of a variety of cell types; a part of osteosarcoma cells, fibroblastic cells surrounding osteosarcoma (possibly including CAFs), CD31-negative cells localized around blood vessels, and CD31/αSMA double-positive cells (Figs. 6A and S2). However, these cells were also abundant in the tumors of nintedanib-treated mice, indicating that nintedanib treatment did not result in quantitative changes in αSMA-positive cells.

A previous report suggested that nintedanib promoted anti-tumor immunity and potentiated the effects of immune checkpoint inhibitors (23). However, tumor-infiltrating CD8-positive T cells were not numerous in either control or nintedanib-treated mice (Fig. 6B). In addition, nintedanib exhibited anti-osteosarcoma activity in C57BL/6 SCID mice, in which T- and B-cell function is obsolete (Fig. 6C and D).

Next, we evaluated the effect of nintedanib on vasculature formation in osteosarcoma. Immunohistochemical staining revealed that nintedanib reduced the formation of CD31-positive ducts, despite the variable abundance of tumor vasculatures (Fig. 7A and B). To evaluate the effect of nintedanib on vascular

formations more directly, endothelial cell tube formation assay was performed. HUVEC formed tubes in 14 h in Matrigel and they became thinner and interrupted by the supplement of nintedanib compared to the control (Fig. 7C and D). Nintedanib treatment also attenuated the viability of HUVEC (Fig. 7E).

These findings indicated that nintedanib exerted anti-tumor activity in our osteosarcoma model mainly by inhibiting tumor vascular formation.

Discussion

In this study, we examined the anti-osteosarcoma effect of nintedanib *in vitro* and *in vivo*. Notably, BMSCs were more sensitive to nintedanib treatment than osteosarcoma AXT cells (Fig. 1A). Previous studies indicate that nintedanib exhibits therapeutic effects in idiopathic pulmonary fibrosis, which is an approved clinical indication of nintedanib, by inhibiting growth factor-induced cell proliferation (35,36). BMSCs might show higher sensitivity to nintedanib via the same growth factor-dependent mechanisms. On the other hand, AXT cells, whose viability is driven by oncogenes, might be less dependent on growth factors than BMSCs. Human osteosarcoma cell lines had different susceptibilities to nintedanib, and MG63 cells were less sensitive than the other cell types (Fig. 1B). Several studies have suggested that cell lines of the same cancer type have different susceptibilities to nintedanib (16-18).
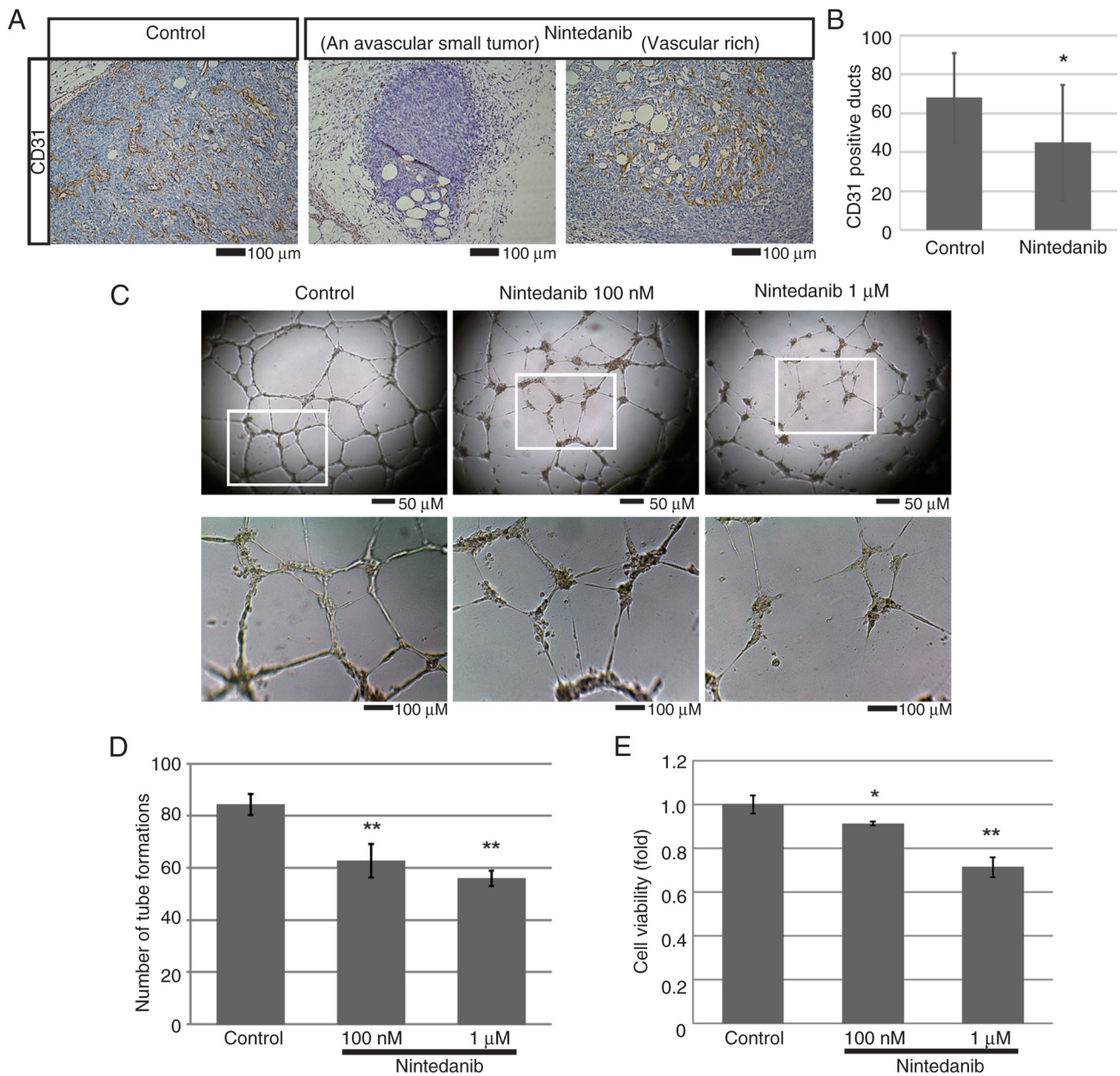
Figure 7. Nintedanib attenuates tumor vascular formations in osteosarcoma. (A) Immunohistochemistry of CD31 in AXT-derived osteosarcoma developed according to the schedule in Fig. 4A. (B) The number of CD31-positive ducts present throughout a randomly sliced section was counted. Data were shown as the mean values ± SD from randomly selected primary tumors from five mice. (C) Representative images of the tube formation assay using HUVEC. Boxed regions highlight the magnified images. (D) The number of tubes in the 4x magnification field was counted. Data were shown as the mean values ± SD from triplicate experiments. (E) The viability of human umbilical vein endothelial cell was measured after 2 day exposure to the indicated concentrations of nintedanib. Data are shown as the means ± SD relative to the corresponding value without nintedanib exposure. *P<0.05. **P<0.005 vs. control.

In AXT cells, nintedanib treatment decreased the S-phase population and induced apoptosis in a concentration-dependent manner (Fig. 2). However, the concentrations of nintedanib needed to produce this effect were much higher than the IC50 value of nintedanib for inhibiting FGFR, PDGFR, and VEGFR, which is less than 150 nM (10). The suppression of signal activation other than its initial targets might be involved in decreasing the S-phase population and inducing apoptosis *in vitro*.

The phosphorylation of AKT was suppressed by nintedanib, while a high concentration re-activated ERK1/2 (Fig. 3B). This paradoxical phenomenon was also observed in human bladder cancer cell lines; the authors of that study suggested that high-concentration nintedanib activates

signals that are independent of those that control cancer cell sensitivity and viability (19). High-concentration nintedanib *in vitro* might activate a complex cross-talk of PI3K, MAPK, and other signaling pathways.

Importantly, single-agent nintedanib suppressed the formation of both primary and metastatic lesions of osteosarcoma (Fig. 4). Since PDGFR activation was inhibited *in vivo* and p-ERK was also attenuated, these findings show that nintedanib inhibited its target molecules *in vivo*. In *in vitro* experiments, nintedanib only inhibited cell growth by 10%, even when AXT cells were continuously exposed to 1 μM of nintedanib for 3 days (Fig. 1A). On the other hand, *in vivo* nintedanib administration reduced tumor size by more than half compared with the control

(Figs. 4C and 6D). These findings suggest that nintedanib exerts a stronger anti-tumor effect *in vivo*. Notably, the nintedanib-mediated inhibition of p-AKT seen *in vitro* was not observed *in vivo* (Fig. 5F). Unlike the *in vitro* environment, the tumor microenvironment consists of complex structures and various cells and factors related to tumor cells (37,38). The continuous activation of AKT that was observed even in the presence of nintedanib is likely due to activation signals from upstream molecules that are not the target molecules of nintedanib (Fig. 5B).

Histological analysis showed that nintedanib significantly suppressed osteosarcoma angiogenesis (Fig. 7A and B). Immunoblot analysis using tumor lysate could not detect the activation of VEGFR, although VEGF is a critical factor for angiogenesis. It is plausible that nintedanib also might block VEGFR activation, which contributes to angiogenesis at levels that were undetectable in this study.

Nintedanib administration did not reduce αSMA-positive cells in osteosarcoma (Figs. 6A and S2). Notably, many tyrosine kinases were still phosphorylated in tumors of nintedanib-treated mice (Fig. 5B). The factors involved in the activation of these kinases might function to maintain the enrichment of CAFs. For instance, EphA3 was shown to be important for the recruitment of CAFs in a mouse lung cancer model (39). The constitutive activation of JAK1was suggested to confer sustained proinvasive ability to CAFs (40).

A previous study showed that nintedanib blocked FGFR-mediated fibrogenic reprogramming of osteosarcoma cells that conferred metastatic ability to primary tumor cells (26). This study clearly demonstrated that originally Fibronectin (FN)/αSMA-negative Well5 cells in the primary bone lesion were changed to FN/αSMA-positive cells during metastatic process through the activation of FGFR signaling. Our previous study also suggests that FGF2 released from the tumor environment suppresses osteogenesis and promotes proliferation and migration of osteosarcoma cells (9). However, regarding the fibrogenic properties, unlike Well5 cells, the primary lesions already contained a lot of αSMA-positive osteosarcoma cells (Fig. 6A), suggesting that AXT osteosarcoma cells in primary lesions originally possess highly malignant properties without the need for FGFR signaling.

Collectively, the results of this study showed that nintedanib has a direct anti-tumor effect on osteosarcoma at concentrations higher than those to block its initial targets *in vitro*, and more importantly, suppresses osteosarcoma progression *in vivo*. Nintedanib possibly exerts anti-osteosarcoma effect by modulating the tumor environment rather than directly targeting tumor cells. Therefore, nintedanib could be an effective option for refractory osteosarcoma.

Availability of data and materials

The data generated in the present study may be requested from the corresponding author.

Authors' contributions

TS, AS and AM confirm the authenticity of all the raw data. TS contributed to conceptualization, design, acquisition of data, data curation, formal analysis, funding acquisition, investigation, methodology, project administration, validation, visualization and original draft preparation. AS contributed to data curation, statistical analysis, analysis and interpretation of data, and reviewing and editing. YF contributed to acquisition of data. AM contributed to analysis and interpretation of data, supervision and administrative support. All authors have read and approved the final manuscript.

Ethics approval and consent to participate

All animal care and procedures were performed in accordance with the guidelines of Hoshi University, and the present study was approved by the Committee on Animal Research of Hoshi University (approval number: 20-071).

Patient consent for publication

Not applicable.

Competing interests

The authors declare that they have no competing interests.

References

1. Ritter J and Bielack SS: Osteosarcoma. Ann Oncol 21 (Suppl 7): vii320-vii325, 2010.
2. Fletcher CDM, Unni KK and Mertens F (eds): Osteogenic tumours: WHO Classification Tumours of Soft Tissue and Bone. IARC Press, Lyon, 2002.
3. Jaffe N: Osteosarcoma: Review of the past, impact on the future. The American experience. Cancer Treatment and Res 152: 239-262, 2009.
4. Moore DD and Luu HH: Osteosarcoma. Cancer Treat Res 162: 65-92, 2014.
5. Shimizu T, Ishikawa T, Sugihara E, Kuninaka S, Miyamoto T, Mabuchi Y, Matsuzaki Y, Tsunoda T, Miya F, Morioka H, *et al*: c-MYC overexpression with loss of Ink4a/Arf transforms bone marrow stromal cells into osteosarcoma accompanied by loss of adipogenesis. Oncogene 29: 5687-5699, 2010.
6. Shimizu T, Sugihara E, Yamaguchi-Iwai S, Tamaki S, Koyama Y, Kamel W, Ueki A, Ishikawa T, Chiyoda T, Osuka S, *et al*: IGF2 preserves osteosarcoma cell survival by creating an autophagic state of dormancy that protects cells against chemotherapeutic stress. Cancer Res 74: 6531-6541, 2014.
7. Yamaguchi SI, Ueki A, Sugihara E, Onishi N, Yaguchi T, Kawakami Y, Horiuchi K, Morioka H, Matsumoto M, Nakamura M, *et al*: Synergistic antiproliferative effect of imatinib and adriamycin in platelet-derived growth factor receptor-expressing osteosarcoma cells. Cancer Sci 106: 875-882, 2015.
8. Kamel WA, Sugihara E, Nobusue H, Yamaguchi-Iwai S, Onishi N, Maki K, Fukuchi Y, Matsuo K, Muto A, Saya H and Shimizu, T: Simvastatin-induced apoptosis in osteosarcoma cells: A key role of RhoA-AMPK/p38 MAPK signaling in antitumor activity. Mol Cancer Ther 16: 182-192, 2017.

9. Shimizu T, Ishikawa T, Iwai S, Ueki A, Sugihara E, Onishi N, Kuninaka S, Miyamoto T, Toyama Y, Ijiri H, et al: Fibroblast growth factor-2 is an important factor that maintains cellular immaturity and contributes to aggressiveness of osteosarcoma. Mol Cancer Res 10: 454-468, 2012.

10. Hilberg F, Roth GJ, Krssak M, Kautschitsch S, Sommergruber W, Tontsch-Grunt U, Garin-Chesa P, Bader G, Zoephel A, Quant J, et al: BIBF 1120: Triple angiokinase inhibitor with sustained receptor blockade and good antitumor efficacy. Cancer Res 68: 4774-4782, 2008.

11. Roth GJ, Heckel A, Colbatzky F, Handschuh S, Kley J, Lehmann-Lintz T, Lotz R, Tontsch-Grunt U, Walter R and Hilberg F: Design, synthesis, and evaluation of indolinones as triple angiokinase inhibitors and the discovery of a highly specific 6-methoxycarbonyl-substituted indolinone (BIBF 1120). J Med Chem 52: 4466-4480, 2009.

12. Wind S, Schmid U, Freiwald M, Marzin K, Lotz R, Ebner T, Stopfer P and Dallinger C: Clinical pharmacokinetics and pharmacodynamics of nintedanib. Clin Pharmacokinet 58: 1131-1147, 2019.

13. Richeldi L, Costabel U, Selman M, Kim DS, Hansell DM, Nicholson AG, Brown KK, Flaherty KR, Noble PW, Raghu G, et al: Efficacy of a tyrosine kinase inhibitor in idiopathic pulmonary fibrosis. New Engl J Med 365: 1079-1087, 2011.

14. Richeldi L, du Bois RM, Raghu G, Azuma A, Brown KK, Costabel U, Cottin V, Flaherty KR, Hansell DM, Inoue Y, et al: Efficacy and safety of nintedanib in idiopathic pulmonary fibrosis. New Engl J Med 370: 2071-2082, 2014.

15. Reck M, Kaiser R, Mellemgaard A, Douillard JY, Orlov S, Krzakowski M, von Pawel J, Gottfried M, Bondarenko I, Liao M, et al: Docetaxel plus nintedanib versus docetaxel plus placebo in patients with previously treated non-small-cell lung cancer (LUME-Lung 1): A phase 3, double-blind, randomised controlled trial. Lancet Oncol 15: 143-155, 2014.

16. Kutluk Cenik B, Ostapoff K T, Gerber DE and Brekken RA: BIBF 1120 (nintedanib), a triple angiokinase inhibitor, induces hypoxia but not EMT and blocks progression of preclinical models of lung and pancreatic cancer. Mol Cancer Ther 12: 992-1001, 2013.

17. Awasthi N and Schwartz RE: Profile of nintedanib in the treatment of solid tumors: The evidence to date. Onco Targets Ther 8: 3691-3701, 2015.

18. Awasthi N, Hinz S, Brekken RA, Schwarz MA and Schwarz RE: Nintedanib, a triple angiokinase inhibitor, enhances cytotoxic therapy response in pancreatic cancer. Cancer Lett 358: 59-66, 2015.

19. Marqués M, Corral S, Sánchez-Díaz M, Del Pozo N, Martínez de Villarreal J, Schweifer N, Zagorac I, Hilberg F and Real FX: Tumor and stromal cell targeting with nintedanib and alpelisib overcomes intrinsic bladder cancer resistance. Mol Cancer Ther 22: 616-629, 2023.

20. Liu J, Gao J, Wang A, Jiang Z, Qi S, Qi Z, Liu F, Yu K, Cao J, Chen C, et al: Nintedanib overcomes drug resistance from upregulation of FGFR signalling and imatinib-induced KIT mutations in gastrointestinal stromal tumours. Mol Oncol 16: 1761-1774, 2022.

21. Gabasa M, Ikemori R, Hilberg F, Reguart N and Alcaraz J: Nintedanib selectively inhibits the activation and tumour-promoting effects of fibroblasts from lung adenocarcinoma patients. Br J Cancer 117: 1128-1138, 2017.

22. Yamanaka T, Harimoto N, Yokobori T, Muranushi R, Hoshino K, Hagiwara K, Gantumur D, Handa T, Ishii N, Tsukagoshi M, et al: Nintedanib inhibits intrahepatic cholangiocarcinoma aggressiveness via suppression of cytokines extracted from activated cancer-associated fibroblasts. Br J Cancer 122: 986-994, 2020.

23. Kato R, Haratani K, Hayashi H, Sakai K, Sakai H, Kawakami H, Tanaka K, Takeda M, Yonesaka K, Nishio K and Nakagawa K: Nintedanib promotes antitumour immunity and shows antitumour activity in combination with PD-1 blockade in mice: Potential role of cancer-associated fibroblasts. Br J Cancer 124: 914-924, 2021.

24. Ledermann JA, Hackshaw A, Kaye S, Jayson G, Gabra H, McNeish I, Earl H, Perren T, Gore M, Persic M, et al: Randomized phase II placebo-controlled trial of maintenance therapy using the oral triple angiokinase inhibitor BIBF 1120 after chemotherapy for relapsed ovarian cancer. J Clin Oncol 29: 3798-3804, 2011.

25. Grosso F, Steele N, Novello S, Nowak AK, Popat S, Greillier L, John T, Leighl NB, Reck M, Taylor P, et al: Nintedanib plus pemetrexed/cisplatin in patients with malignant pleural mesothelioma: Phase II results from the randomized, placebo-controlled LUME-meso trial. J Clin Oncol 35: 3591-3600, 2017.

26. Zhang W, Zhao JM, Lin J, Hu CZ, Zhang WB, Yang WL, Zhang J, Zhang JW and Zhu J: Adaptive fibrogenic reprogramming of osteosarcoma stem cells promotes metastatic growth. Cell Rep 24: 1266-1277.e5, 2018.

27. Shimizu T, Kimura K, Sugihara E, Yamaguchi-Iwai S, Nobusue H, Sampetrean O, Otsuki Y, Fukuchi Y, Saitoh K, Kato K, et al: MEK inhibition preferentially suppresses anchorage-independent growth in osteosarcoma cells and decreases tumors in vivo. J Orthop Res 39: 2732-2743, 2021.

28. Shimizu T, Sugihara E, Takeshima H, Nobusue H, Yamaguchi R, Yamaguchi-Iwai S, Fukuchi Y, Ushijima T, Muto A and Saya H: Depletion of R270C mutant p53 in osteosarcoma attenuates cell growth but does not prevent invasion and metastasis in vivo. Cells 11: 3614, 2022.

29. Schneider CA, Rasband WS and Eliceiri KW: NIH image to ImageJ: 25 Years of image analysis. Nat Methods 9: 671-675, 2012.

30. Johnson DE, O'Keefe RA and Grandis JR: Targeting the IL-6/JAK/STAT3 signalling axis in cancer. Nat Rev Clin Oncol 15: 234-248, 2018.

31. Ha H, Debnath B and Neamati N: Role of the CXCL8-CXCR1/2 axis in cancer and inflammatory diseases. Theranostics 7: 1543-1588, 2017.

32. Gross AC, Cam H, Phelps DA, Saraf AJ, Bid HK, Cam M, London CA, Winget SA, Arnold MA, Brandolini L, et al: IL-6 and CXCL8 mediate osteosarcoma-lung interactions critical to metastasis. JCI Insight 3: e99791, 2018.

33. Sappino AP, Skalli O, Jackson B, Schürch W and Gabbiani G: Smooth-muscle differentiation in stromal cells of malignant and non-malignant breast tissues. Int J Cancer 41: 707-712, 1988.

34. Orimo A, Gupta PB, Sgroi DC, Arenzana-Seisdedos F, Delaunay T, Naeem R, Carey VJ, Richardson AL and Weinberg RA: Stromal fibroblasts present in invasive human breast carcinomas promote tumor growth and angiogenesis through elevated SDF-1/CXCL12 secretion. Cell 121: 335-348, 2005.

35. Wollin L, Maillet I, Quesniaux V, Holweg A and Ryffel B: Antifibrotic and anti-inflammatory activity of the tyrosine kinase inhibitor nintedanib in experimental models of lung fibrosis. J Pharmacol Exp Ther 349: 209-220, 2014.

36. Hostettler KE, Zhong J, Papakonstantinou E, Karakiulakis G, Tamm M, Seidel P, Sun Q, Mandal J, Lardinois D, Lambers C and Roth M: Anti-fibrotic effects of nintedanib in lung fibroblasts derived from patients with idiopathic pulmonary fibrosis. Respir Res 15: 157, 2014.

37. Labrie M, Brugge JS, Mills GB and Zervantonakis IK: Therapy resistance: Opportunities created by adaptive responses to targeted therapies in cancer. Nat Rev Cancer 22: 323-339, 2022.

38. Bejarano L, Jordão MJC and Joyce JA: Therapeutic targeting of the tumor microenvironment. Cancer Discov 11: 933-959, 2021.

39. Vail ME, Farnsworth RH, Hii L, Allen S, Arora S, Anderson RL, Dickins RA, Orimo A, Wu SZ, Swarbrick A, et al: Inhibition of EphA3 expression in tumour stromal cells suppresses tumour growth and progression. Cancers (Basel) 15: 4646, 2023.

40. Albrengues J, Bertero T, Grasset E, Bonan S, Maiel M, Bourget I, Philippe C, Herraiz Serrano C, Benamar S, Croce O, et al: Epigenetic switch drives the conversion of fibroblasts into proinvasive cancer-associated fibroblasts. Nat Commun 6: 10204, 2015.